Analysis of mechanical properties of a lattice structure produced with the additive technology

Analysis of mechanical properties of a lattice structure produced with the additive technology

Jozef Tkac[a], Sylwester Samborski[b,*], Katarina Monkova[a,c], Hubert Debski[d]

[a]*Faculty of Manufacturing Technologies with Seat in Presov, Technical University of Kosice, Sturova 31, 080 01 Presov, Slovak Republic*

[b]*Faculty of Mechanical Engineering, Department of Applied Mechanics, Lublin University of Technology, Nadbystrzycka 36, 20-618 Lublin, Poland*

[c]*Faculty of Technology, UTB Tomas Bata University in Zlin, Vavreckova 275, 76001 Zlin, Czech Republic*

[d]*Faculty of Mechanical Engineering, Department of Machine Design and Mechatronics, Lublin University of Technology, Nadbystrzycka 36, 20-618 Lublin, Poland*

[*]*Corresponding author. E-mail address: s.samborski@pollub.pl (S. Samborski).*

ABSTRACT

Mechanical characteristics of 3D printed lattice structures primarily depend on the properties of materials from which they are produced. Another factor is the topology of the structure. In the paper it was shown, that the behavior of the lattice can significantly differ from the fully-dense material and both the experiments and the FE modelling is necessary to describe well the structure in the macroscopic sense. A separate problem is damage identification along with the process of deformation - this however can be done with satisfactory effect by treating the lattice as a porous structure. For creating the 3D model of the lattice/porous structure the PTC Creo 6 CAD software was used. It enabled both physical realization of the porous ABS specimens and exporting the geometry to the FE software environment Abaqus. The performed experimental tests of uniaxial compression enabled determination of the material model necessary to be implemented in the numerical simulations. The macroscopic damage initiation and its evolution was described well with a scalar damage parameter. The proposed procedure might be accepted as a simple and easy-to-implement methodology for the assessment of the lattice/porous material deterioration.

Keywords: 3D printing, lattice structure, porous structures, finite element, compression, damage, lightweight materials

1. Introduction

By reducing costs and making production more efficient, lightweight materials with good mechanical properties are used in technical practice, where the most important prosperity is their advantageous ratio of compressive strength to mass density [**1**]. The development of 3D printing technology is nowadays possible for the production of such structures metallic and non-metallic materials. Possibilities of using porous structures are mainly in the automotive and aerospace industry, but also in various sectors of the economy [**2**]. The 3D printed elements have a lattice structure, with internal voids and as such can be thought of and in consequence modeled as porous or foam materials, depending on the level of their porosity.

The properties of these materials offer multiple applications of porous structures where it would be difficult to use conventional materials. In order to avoid premature damage and thus failure of the entire equipment, the component must meet the specific criteria for damage tolerance [**3**]. The issues of the porous structures are currently solved by a number of researchers whose focus their interest not only into mechanical but also the physical properties of several types of porous bodies made of different materials.

Buj-Corral et al. [**4**] dealt with the problem of 3D printing of porous structures with different porosity and pore sizes. The authors presented in their research a new method for the design of porous structures produced through additive manufacturing. The designed geometrical model consists of parallel layers with several pillars of a specific radius. Jorge et al. [**5**] investigated laminar flow characteristics in porous structures that had open cells. Study dealt with the numerical analysis of 3D flow by periodic porous structures. During the research it was found that the cell orientation and tortuosity did not affect the Darcy coefficient due to their mutual negation. The experiment showed higher accuracy of Darcy coefficient compared to coefficients published in other studies.

Zaharin et al. [**6**] examined the effect of cell type and pore size on the porosity and mechanical behavior of components made of titanium alloy (Ti-6Al-4V) by additive technology. Hanzl [**7**] dealt with the influence of the volume ratio of a certain type of porous structures, made by DMLS steel technology on its load-bearing capacity. His publication revealed a relationship between the volume fraction of the entire structure and the load-bearing capacity of the gyroid structure. Hussein [**8**] studied the manufacturing and mechanical behavior of advanced lightweight cellular structures produced by metallic additive technology. In his research, he used cell structures that were based on a three-periodic minimal surface cell (TPMS) typology. Complex experimental tests were performed for various cell topologies using commercially available 316L stainless steel, titanium alloy (Ti-6Al-4V) and aluminum alloy metal powders (AlSi10Mg).

The Mechanical behavior of advanced lightweight cellular structures has also been investigated by Fedorko et al. in their research to failure analysis for steel cord conveyor belts [**9**]. Hao et al. [**10**] made the experiments with the production of complex porous metal structures using SLM technology. The regular diamond and gyroid structures at different cell sizes were modeled using implicitly assigned mathematical equations. The results showed that the generation of structures that are mathematically defined is very accurate and flexible. In production, it has been shown that both types of structures with a cell size of 2, 5 and 8 mm could be produced without any deformation.

The study of Yan et al. [**11**] was focused on the production of a gyroid structure. Several test specimens with varying volume ratio have been made to produce the structures. Samples with cell sizes of 2-8 mm have been reliably manufactured by metallic additive technology with good shape conformance comparing to a virtual model. The tests proved that along with increasing the base cell size the strength of the structure decreases.

Aremu et al. [**12**] investigated mechanical properties of self-supporting structures produced with the selective laser melting (SLM) technology, demonstrating that the mechanical properties of the structure are strongly dependent on cell topology. Several types of selfsupporting structures were tested, including a gyroid structure, and it was found that gyroid structures in some cases achieved the same mechanical properties as those of self-supporting structures.

The study of Zhang et al. [**13**] dealing with boemite gel foams made by 3D printing brought the new hierarchical porous foams which had superior strength and high porosity. Due to the high printability, gel foams turned out to be an ideal material for 3D printing. Excellent printability due to its predominant stability, high yield stress and storage modulus has also been investigated in research by

Kulka et al. [**14**]. Kohnen et al. [**15**] dealt with the mechanical properties and deformation behavior of lattice structures made of stainless steel by the additive technology. They used the SLM technology to create two different types of lattice structures. These structures demonstrated the equal unique energy absorption with comparison to the full-volume reference samples. Lozanovski et al. [**16**] presented a study, Computational modelling of strut defects in SLM manufactured lattice structures. Their research gave the manufacturing defects elements of the strut of a porous structure, thus enhancing the capabilities of models.

Lang et al. [**17**] dealt with construction of YSZ porous ceramics with precise porosity control. Current preparation of porous ceramics usually hard to exactly control the porosity of the samples. In their research, the foaming process was fixed in a defined area of the ball-mill tank and porous ceramics with diverse porosity were reached by varying the amount of slurry. The results showed that the porosity of the sample varied linearly with the inflation when slurry was added. Samborski and Sadowski [**18**] provided a study deals with theoretical foundations of micromechanical constitutive modeling of porous polycrystalline ceramic materials under compression. The deformation process includes elastic phase, dislocation band creation, microcrack initiation and finally - the crack-development phase, leading to crack kinking and failure of a specimen. Prediction of the mechanical behavior of porous ceramics in mesoscale was another investigation by Sadowski and Samborski [**19**]. In the work a mesomechanical modelling of porous polycrystalline ceramics subjected to different kinds of loading is presented with two different crack initiation mechanisms on account of stress concentration at the pore boundary. The analyses of deformation were performed both in tension and compression. As shown by the authors, in polycrystalline ceramic material cracks grow mainly intergranularly due to a lower value of the fracture toughness of the grain boundary in comparison to the one of the grains. In another article [**20**], Sadowski and Samborski investigated different response of porous polycrystalline ceramic materials under uniaxial tension and compression of porous aluminum oxide (Al_2O_3). In both stress states the proposed approach of damage description reflected well the gradual changes of mechanical features. The experimental study [**21**] revealed a predictive ability of damage description method provided by Samborski and Sadowski, bases on the tracking of continuous changes in the stiffness of porous structures along with damage evolution.

Development of damage state in porous ceramics under compression was conducted by Sadowski et al. [**22**]. A loading history called loading-unloading-reloading Procedure (LURP) was applied during experimental testing. Numerical results demonstrated that the proposed method is a good approximation of the real behavior of ceramics experienced a progressive damage. Their approach for damage evolution description has been successfully applied in the current article, as shown farther in **Section 3**.

As observed by Kubiak et al. [**23**] the methods for monitoring damage initiation and evolution in real time, such as the acoustic emission (AE) technique, can be very useful in laboratory practice. As shown by the authors the AE equipment enabled detection and identification of various defects developing inside the composite profiles under compression prior to any visible or audible symptoms of material deterioration.

Tandon et al. [**24**] published the first ever review of vibration and acoustic measurement methods to detect defects in rolling elements of bearings. Detection of both distributed and localized defects was examined. A definition for the noise and vibration generation in bearings was formulated. Frequency domains and vibration measurement in both times using signal processing techniques such as the high-frequency resonance technique have been enclosed. Comparison of vibration and acoustic measurement techniques for the condition monitoring of rolling element bearings was investigated by Tandon et al. [**25**]. The measurements were conducted on the new bearings, as well as the bearings

with simulated defects in their elements. The results showed that the disclosure of defects with acoustic emission is improved as compared to other measurements.

Chan et al. [**26**] investigated robust topology optimization of multimaterial lattice structures under material and load uncertainties. This study presented a robust topology optimization method for multi-material porous structures under any combination of material and load uncertainties. The method applied a new material interpolation scheme for an erratic number of materials and occupies univariate dimension contraction. The study, Topological phase and lattice structures in spin-chain models was performed by Li et al. [**27**]. The researchers studied the topological property based on several proposed related models. They showed that the topologically nontrivial phase in the model of lattice structure could exist under other model conditions and could even be caused by material anisotropy. It is element has a close affiliation with the even-bond dimerization. This conclusion declares the topological invariant of the system and might afford extended topological materials for experimental analysis. Jin et al. [**28**] dealt with failure and energy absorption characteristics of four lattice structures under dynamic loading. Their results proved that the mechanical properties of the lattice structures with disparate relative density could be characterized by a power function. This demonstrates that lattice structures with the deformation mode illustrate better mechanical properties under dynamic loading. Fracture characteristic analysis of cellular lattice structures under tensile load was investigated by Geng et al. [**29**]. This study showed a simulation process consisting of a finite element method and numerical results predicted by this method. The simulation results revealed new possible damage scenarios associated with the experimental results.

Also Samborski and Sadowski [**30**] dealt with dynamic fracture toughness estimation for porous ceramics. Their paper presents a comparison of experimental results of a dynamic stress intensity factor (K_{id}) and its static counterpart (K_{ic}). The tests were performed for two kinds of porous ceramics (Al_2O_3 and MgO) with various porosity fraction. it was found that the increase in initial porosity reduced values of both static and dynamic fracture characteristic, even though the values of KId were higher at any porosity level.

Zargarian et al. [**31**] were interested in the fatigue behavior of additive manufactured lattice structures. in their article, the impact of various factors on the fatigue failure of the lattice structure produced by high-cycle additive technology was discussed. The analysis was performed by numerical simulation and the results were compared to experiments. The results of this study pointed to the need for a large number of experiments to determine reliable fatigue properties of cellular materials.

Thus, the current article deals with the research of the influence of the volume ratio of the material on a behavior of the beam with the lightweight lattice/porous structure.

2. Materials and methods

2.1. Test samples

The ABSplus-P430 (Ivory colour) as a built material and P400SR (soluble at 70 °C by means of the SR-100 solution) as supporting structures material were used for the samples production within the presented research. The properties of the raw plastic material ABSplus-P430 are shown in **Table 1**.

The 3D models of the samples were created in PTC Creo 6 software. The basic cell was designed as BCC (Body-Cubic Centered) type with 10 x 10 x 10 mm sizes, as it is presented in **Fig. 1** a). The diameter of a strut is 4 mm. The basic cell was regularly patterned in all three x, y and z directions so that the total sizes of the sample were 70 x 80 x 60 mm.

The volume ratio V [%] of the sample was computed based on the equation:

$$V = \frac{V_{structure}}{V_{total}} * 100\,\% \qquad (1)$$

where, $V_{structure}$ is the volume of the raw ABS material used at the structure building, [mm^3] and V_{total} is the total volume of the sample [mm^3].

In the particular case given in **Fig. 1**:

$$V = \frac{233\,274.42}{336\,000} * 100 = 69.42\,\%$$

The uPrint SE printer (**Fig. 2**) working on the FDM (Fused Deposition Modeling) principle was used for the sample production. The support structures were dissolved in hot water containing the SR-100 solution and small particles of so-called "dust" that was added due to faster dissolving a large ratio of support structures.

2.2. Experimental procedures

The fabricated porous specimens were subjected to a full range (up to failure) compression tests on the Zwick Z100 testing machine, shown on **Fig. 3**, in the laboratories of the Department of Applied Mechanics at Lublin University of Technology (Lublin, Poland). The preliminary stiffness tests were led on a table-top Shimadzu AGS-X machine.

Table 1 The properties of ABSplus-P430 Ivory.

(Tensile) Strength limit R_m	37 MPa
Elongation at break ΔL	4.4
Tensile modulus (Young's modulus) E	1920 MPa
Yield strength Re	37 MPa
Poisson coefficient ν	0.394
Mass density ρ	1.04 g/cm^3

In the **Table 2** basic technical parameters of the main testing machine Zwick/ Z100 are given. Note, that the compression tests were displacement-driven at the traverse velocity set to 1 mm/min, i.e. quasistatically.

The compression tests were led until complete failure of the specimens (**Figs. 4 and 5**).

Concerning damage monitoring, a threefold observation was applied:

- visual observation of the specimens to spot the first crack revealing at the outer surface,
- digital image correlation (DIC) analysis with the GOM/Aramis system,
- acoustic emission (AE) detection of the first damage phenomenon during compression with the Vallen/AMSY-5 equipment.

The application of DIC explains the reason for the specimen painting seen in **Fig. 4**. The figure also includes the acoustic emission sensor Fujicera 1045S, which was used to record the AE data during the compression test.

The compression tests were performed on three the same cubic specimens of dimensions 70 x 80 x 60 mm in the X, Y and Z directions, respectively. However, each of the specimens was compressed in different direction (X, Y or Z - see the marks in **Fig. 1**c)).

The experimental samples before a) and after b) pressure test is presented in **Fig. 5**.

3. FE simulations methodology

Auxiliary compression tests performed on 3 specimens in the three principal directions X, Y and Z within the elastic deformation range (up to 4 kN, with no permanent strains) revealed congruous stiffness of the specimens in any of the three mutually perpendicular directions.

In consequence, the material was modelled as isotropic-plastic with subsequent damage (**Fig. 6**) in the FE analyses, which were one of the fundamental research stages of description of the porous structure behavior in compression. The basic shape of the specimen was drawn with the PTC Creo Parametric software and subsequently imported to the ABAQUS® commercial FE code, enabling complex nonlinear numerical analyses. The elaborated discrete model of the porous ABS specimen is shown in **Fig. 6**.

Discretization (meshing) of the analyzed structure of the porous material was performed using the tetragonal finite elements C3D10 - a ten-node, second order and full integration elements. It has 3 translational and DOFs in each node. The accepted method of the FE mesh construction was the only one possible, because of the complicated macro-structure of the porous specimens. In result of discretization process the numerical model composed of 632,136 nodes and 396,137 finite elements was obtained. The computational task was to solve 1,894,983 nonlinear equations, taking into account contact problems.

The respective boundary conditions were defined through restraining the bottom-surface nodes from translations in the X direction, as well as blocking the Y and the Z translations of a one corner node. The reference point (RF) was allowed to move only along the X axis (global). The load was applied in accordance with the experiment, i.e. the displacement of the reference point along the X axis was quasistatically changing from zero to its maximum - U_x = -2.5 mm. The value of the displacement was uniformly transferred to all the nodes at the top surface of the model through the RF's kinematic interaction with them. The details of the boundary conditions etc. are presented in **Fig. 7**.The performed numerical calculations had a geometrically nonlinear nature. The problem was solved with the incremental-iterative Newton-Raphson method. The accepted computational procedure enabled considering significant displacements and strains of the porous structure in compression. In the definition of the numerical model, contact interactions were introduced as the General contact option, which simulated any internal contacts within the model in the normal directions.

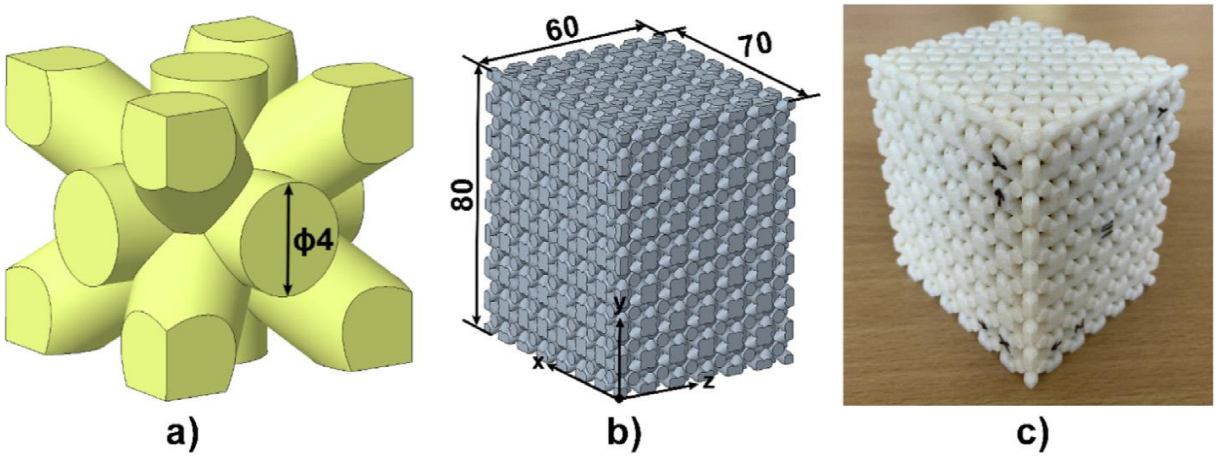

Fig. 1. Basic cell a), 3D model b), experimental sample c).

Fig. 2. The uPrint SE printer.

The material model was defined on the basis of the experimental (1D compression) results as the elastic-plastic one with damage. The experimentally determined stress-strain characteristic was implemented into the ABAQUS® software environment with the appropriate built-in material calibration procedure. The obtained material model was a specific “homogenization” of the mechanical characteristics of the porous ABS in three directions, as no significant anisotropy was observed during the preliminary experiments performed within the elastic deformation range.

4. Results and discussion

4.1. Experimental data reduction scheme

After collecting the experimental results the following data reduction scheme was applied. As seen in **Fig. 8** the raw load-displacement plot obtained during the compression tests with the Zwick Z100 machine exhibited a false nonlinearity in the beginning of the test, what was a typical phenomenon caused by the grips alignment etc. This outset of the curve had to be linearized in order to gain the data needed in the subsequent FE modeling of the material behavior. The linearization was based on the straight part of the load-displacement curve -between the 20kN and 40kN, see **Fig. 9**. The calculated Young modulus of the ABS lattice/porous structure was E_0 = 427.58 MPa (concerning the original experimental data); linear fit gave an approximated value of 425 MPa.

Fig. 3. Testing machine Zwick/Z100.

Table 2 Technical parameters of the testing machine Zwick/Z100 [**32**].

Maximum testing force F_N (tension, compression)	100 kN
Traverse speed	0.0005 ÷ 750 mm/min
Accuracy of set rate	$0.003\%V_{nom}$
Measurement of force within the range from 0.4 to 100% F_{nom}	Class 1
Measurement of force within the range from 2 to 100% F_{nom}	Class 0.5
Initial measurement length of extensometer	11 ÷ 50 mm

Other material constants necessary in the FE modelling are visualized in **Figs. 9 and 10**. In particular, the yield (plastic) limit was found to be equal σ_{yield} = 9.49 MPa at the respective strain value $£_{-yield}$ = 0.0223. The maximum stress, called further the ultimate stress was σ_u = 18.09 MPa at the ultimate strain $£_u$ = 0.0758. It was assumed, that after the ultimate point (σ_u, $£_u$) damage process began. This assumption was confirmed with both the AE data and the DIC observations.

This means the side "slices" of the specimens cracked vertically in the middle of their height. The effect of vertical cracking is typical behavior of specimens in compression [**3**]. However, the material under consideration - an ABS foam underwent plastic deformation prior to any cracking.

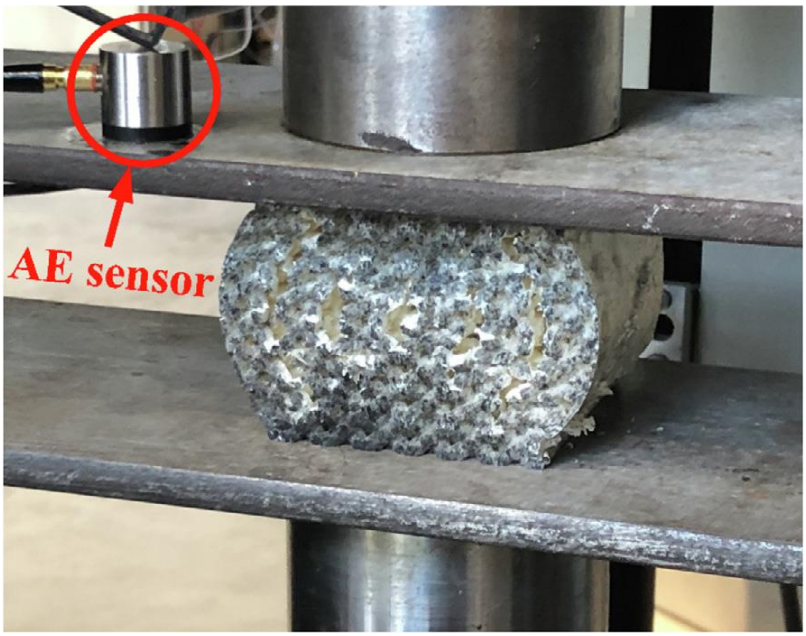

Fig. 4. Compression test of a porous specimen painted for DIC observation with the attached AE sensor.

The current damage state, as well as its evolution in the specimens under compression was described in accordance with the method proposed by Sadowski and Samborski [**3,18-22**]. namely, as it is schematically explained in **Fig. 10**, the secant Young modulus in compression decreased along with damage propagation in the specimen. Damage evolution, starting from the ultimate strain (at which the first crack initiates) can be described with the following damage parameter:

$$D = 1 - \frac{E_{pk}}{E_{ini}} * 100\% \qquad (2)$$

According to this definition damage evolution plot can be constructed (**Fig. 10**) for the propagation values of the secant moduli E_{pk}, with $k \in < 1, n >$. It is assumed that the minimal value of E_{pk} equals E_{ini} - the one at the very moment of crack initiation, and the maximum corresponds to the end (failure point) of the load-displacement curve: $E_{pn} = E_f$.

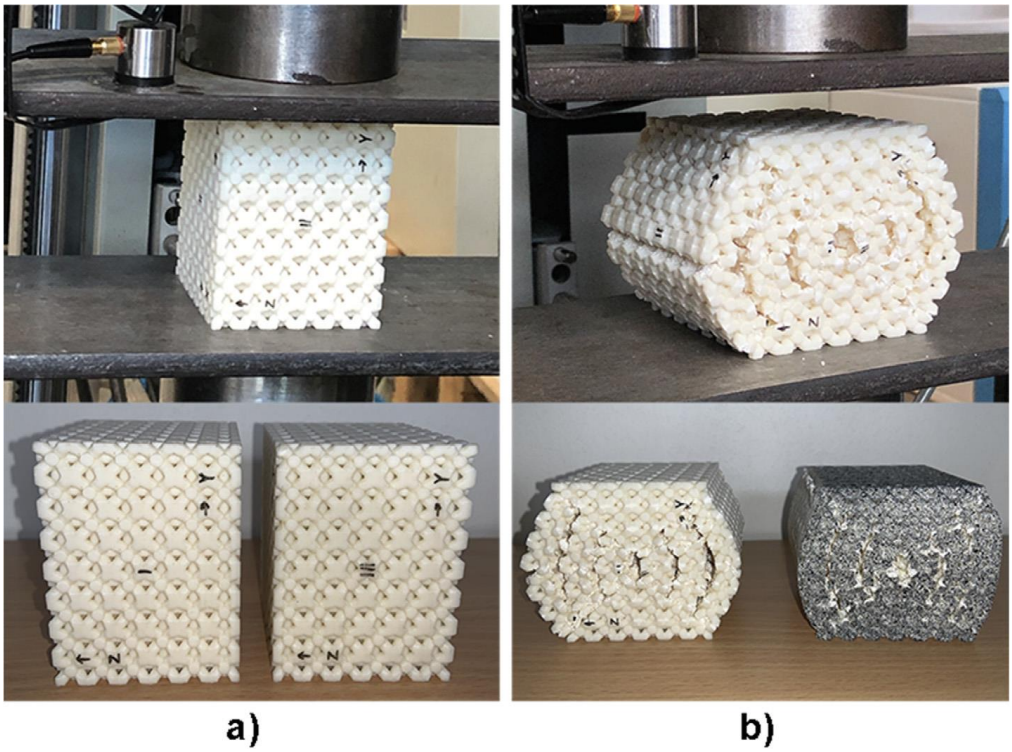

Fig. 5. The experimental samples before (a) and after, (b) compression test.

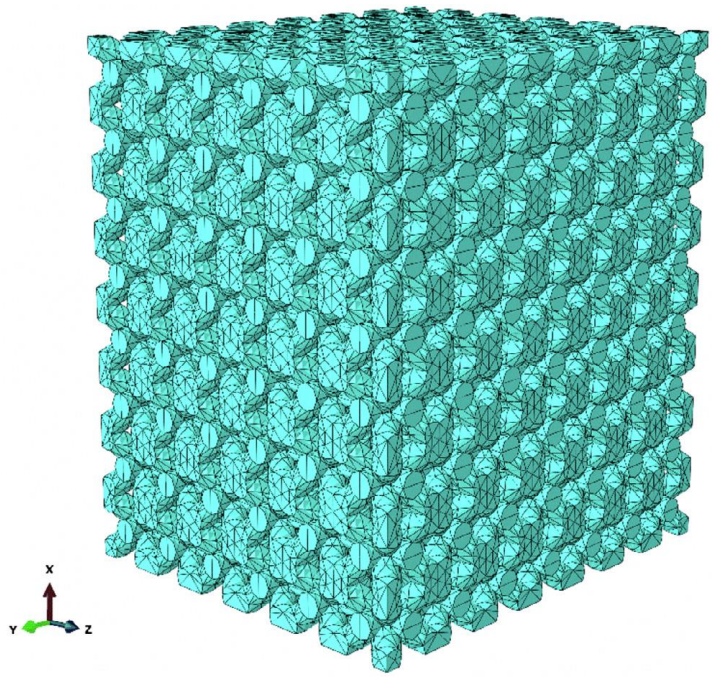

Fig. 6. Numerical model of the analyzed porous ABS - the discretized geometry.

As shown in **Fig. 11**, this approach seems to work well for the lattice structure of 3D printed ABS, even though it was originally used for porous ceramics. In particular, the plot of damage parameter starts from D ≅ 0% at a small strain value (elastic plus plastic) and the line ends at D ≅ 86% which is very close to a commonly accepted teoretical value at failure - D =100%. However, as to the experience of many researchers D hardly ever reaches 100% in real experiments.

4.2. Numerical outcomes based on the experimental data

The numerical simulations enabled determination of the displacement and the principal stress/strain fields inside the structure of the porous material subjected to compression. This obviously wasn't possible in the experiment. In **Fig. 12**, the general maps of the nodal displacements and the principal stresses are provided.

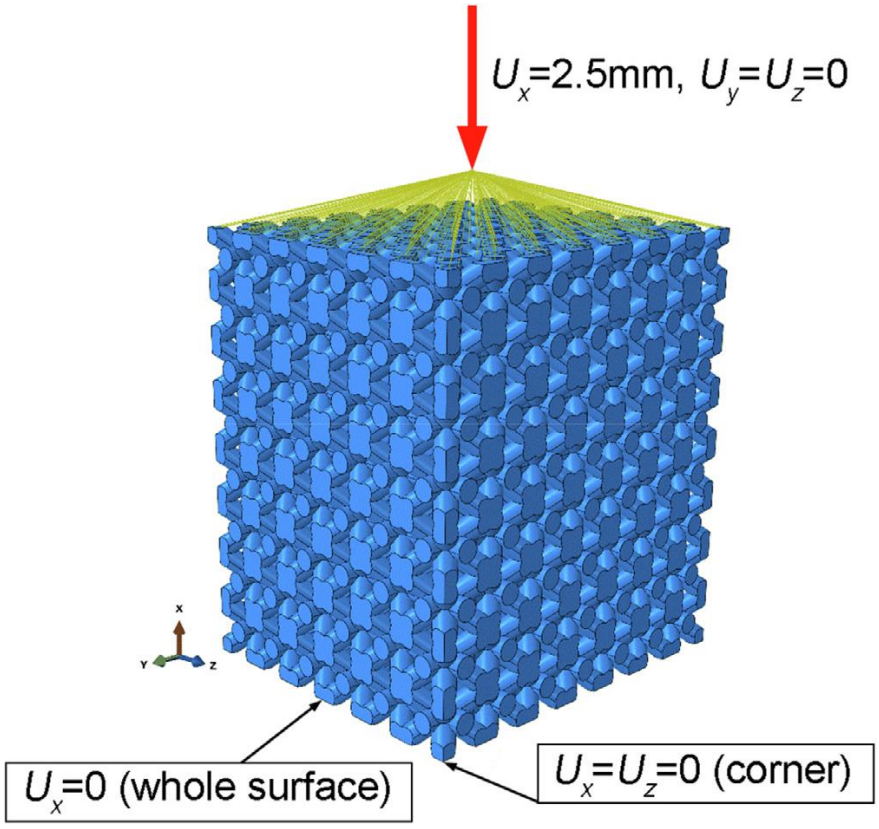

Fig. 7. Boundary conditions and the load application way of the FE model of the porous ABS specimen.

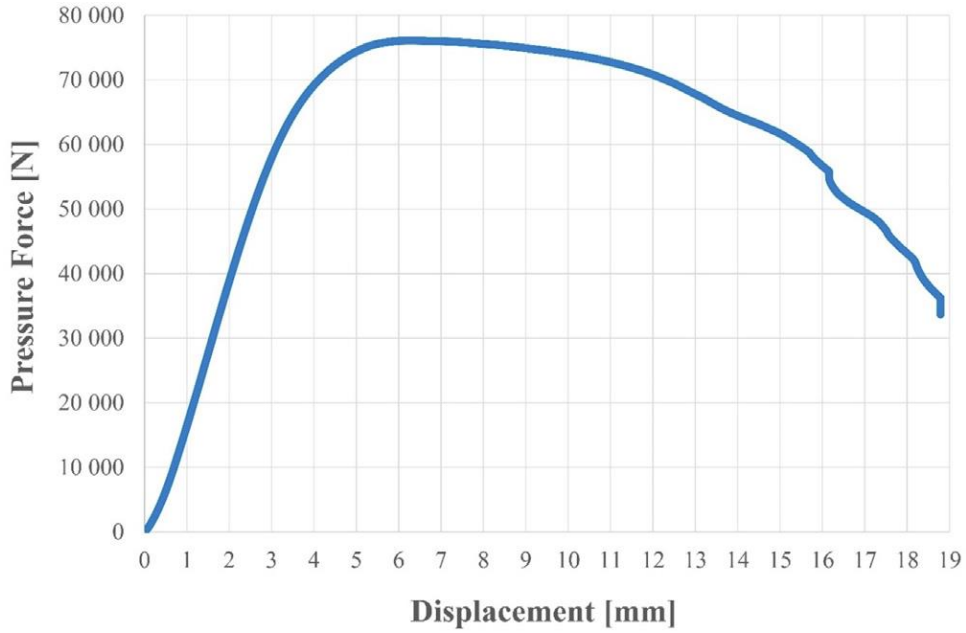

Fig. 8. Dependency of displacement on force.

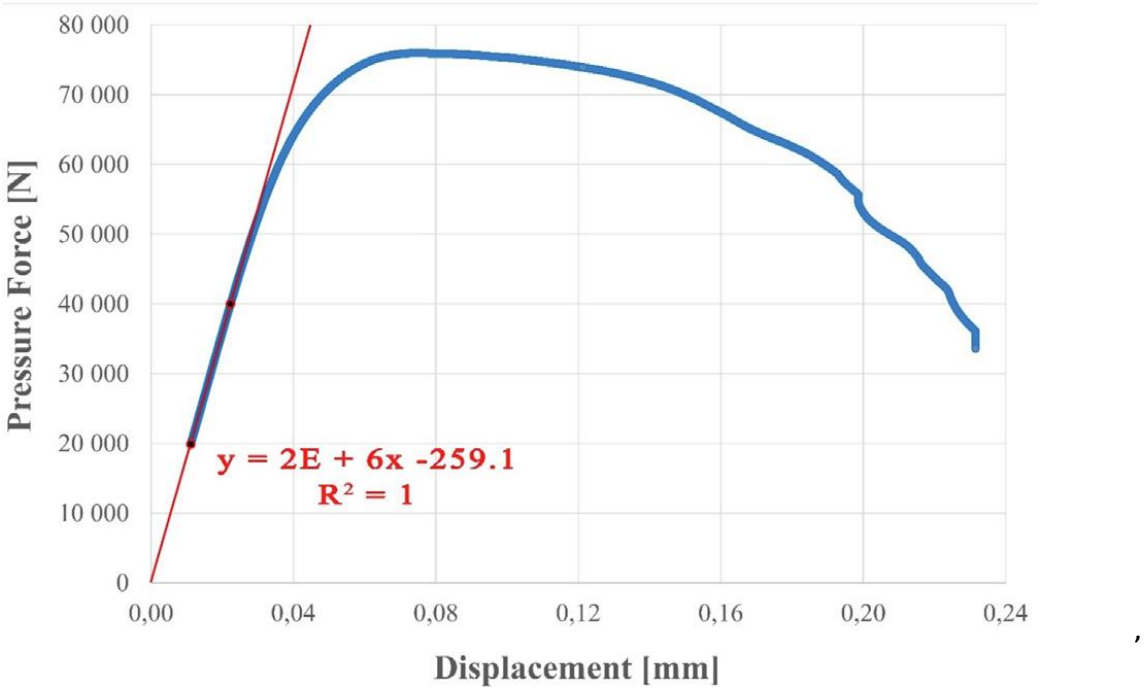

Fig. 9. Linearization of the load-displacement plot.

In order to show the distributions of the principal stresses inside the porous structure - in **Fig. 13** cross-sections of the FE model along the three mutually perpendicular planes of the global coordinate system were revealed.

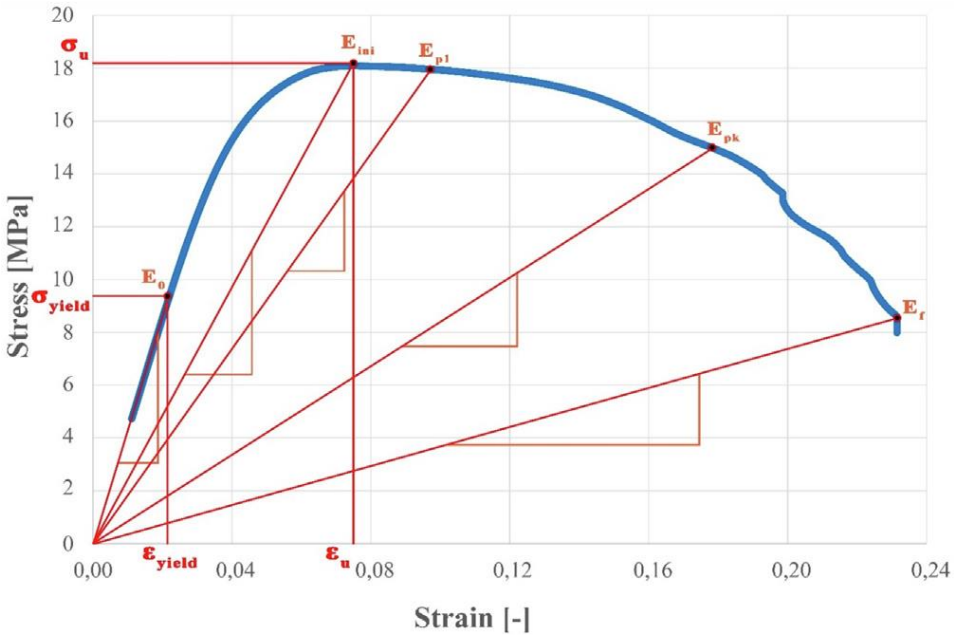

Fig. 10. Damage evolution description scheme.

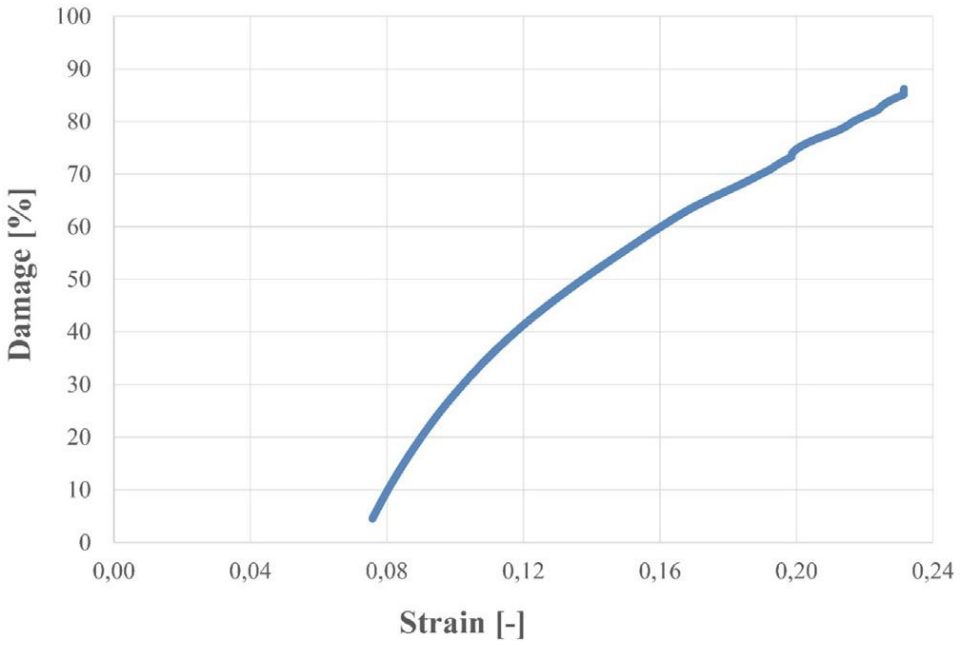

Fig. 11. Damage evolution of the ABS specimen in compression (D vs strain).

The maximal values of the principal stresses reached 13 MPa (in the absolute sense). The obtained maps confirm the supposition that there can be both compressive and tensile stresses iside the porous structure subjected to macroscopic compression. This explains the observed damage mode described below. As shown in **Fig. 13**, the maximal compressive stress pattern regularly in horizontal layers (blue color), whereas tension occurs among the maximal-compression layers. It may result from first of all from the geometry of the porous structure. In addition, for the presented deformation of the structure, i.e. U_x = -2.5 mm the obtained values of both tensile and compressive stress are over the accepted yield stress, σ_{yield} = 9.49 MPa. This means that at a given value of the external load an initiation of the permanent strains can be expected at the stress concentration sites, being further the potential crack

origins, as observed in the experimental compression tests above the stress value au (**Fig. 12**). Nevertheless, the obtained maximal stress values in result of the applied displacement in the numerical model is close to the experimental outcomes: σ_{exp} = 11.5Mpa which means the difference is ca. 12%.

5. Conclusions

In this paper, the FDM technology was used to manufacture a lattice structure with arbitrarily designed geometry. The main goal was to find out how the geometry of the basic cell influenced mechanical characteristics of a sample produced by the additive technology.

The performed experimental tests of uniaxial compression enabled determination of the material model necessary to be implemented in the FE simulations in the Abaqus software.

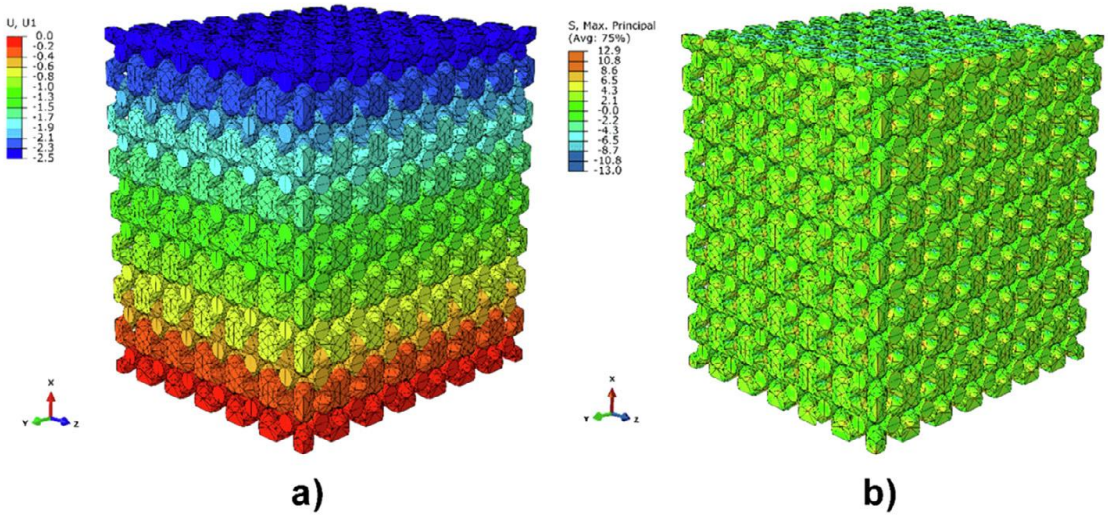

Fig. 12. Results of the numerical simulations: a) nodal displacements [mm], b) principal stresses [MPa].

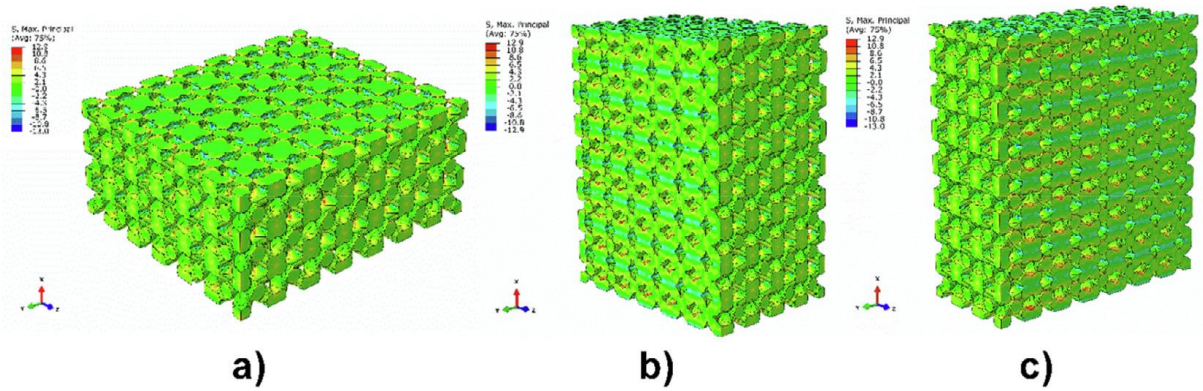

Fig. 13. Internal distributions of the principal stresses in the porous structure: a) the YZ plane, b) the XZ plane, c) the XY plane.

They also revealed the macroscopic damage behavior of the 3D printed lattice ABS structure. The accepted elastic-plastic-damage model was an adaptation of the approach used earlier by one of the authors for porous ceramics. The idea of progressive damage description with a scalar damage parameter - based on the decrease in the secant elastic modulus of the ABS specimens turned out to work well in case of the experimental results. In the FE analyses, based on the experimental outcomes a very good conformity of the model with the real behavior of the material was achieved. The advantage of the numerical simulations in comparison to the stand tests is the possibility to reveal the internal stress and strain fields, which can help in understanding the micromechanics of damage initiation. Further analyses should however take into account a tendency of the lattice ABS structure to form anisotropic damage, even though it was isotropic in the geometrical and material sense.

The proposed procedure for damage description is a simple and easy-to-implement methodology for the assessment of material deterioration and its evolution. The above described research method being the joint analysis of the numerical simulations and the specific experimental data reduction scheme gives good results when applied to lattice/porous structures fabricated with the 3D printing technique.

References

[1] Mišík L, Hloch S, Vagaská A, Monkova K. Side milling factors analysis affecting the surface irregularities of high-grade steel E295. Teh Vjesn 2008;15:19-23.

[2] Monkova K, Monka P, Hloch S. Inverse processing of undefined complex shape parts from structural high alloyed tool steel. Adv Mech Eng 2014;2014. https://doi.org/ 10.1155/2014/478748.

[3] Sadowski T, Samborski S, Librant Z. Damage growth in porous ceramics. Key Eng Mater 2005;290:86-93. https://doi.org/10.4028/www.scientific.net/KEM.290.86.

[4] Buj-Corral I, Bagheri A, Petit-Rojo O. 3D printing of porous scaffolds with controlled porosity and pore size values. Materials (Basel) 2018;11:1-18. https://doi.org/10. 3390/ma11091532.

[5] Jorge P, Mendes MAA, Werzner E, Pereira JMC. Characterization of laminar flow in periodic open-cell porous structures. Chem Eng Sci 2019;201:397-412. https://doi. org/10.1016/j.ces.2019.02.010.

[6] Zaharin HA, Rani AMA, Azam FI, Ginta TL, Sallih N, Ahmad A, et al. Effect of unit cell type and pore size on porosity and mechanical behavior of additively manufactured Ti6Al4V scaffolds. Materials (Basel) 2018;11. https://doi.org/10.3390/ ma11122402.

[7] Hanzl P, Zetek M, Zetková I. Cellular lattice structure produced by selective laser melting and its mechanical properties. In: 26th DAAAM Int. Symp. Intell. Manuf. Autom., vol. 2015-Janua; 2015, p. 748-52. https://doi.org/10.2507/26th.daaam. proceedings.104.

[8] Hussein AY. The development of lightweight cellular structures for metal. Addit Manuf 2013.

[9] Fedorko G, Molnár V, Ferková Ž, Peterka P, Krešák J, Tomašková M. Possibilities of failure analysis for steel cord conveyor belts using knowledge obtained from nondestructive testing of steel ropes. Eng Fail Anal 2016;67:33-45. https://doi.org/10. 1016/j.engfailanal.2016.05.026.

[10] Hao L, Raymont D, Yan C, Hussein A, Young P. Design and additive manufacturing of cellular lattice structures. Innov Dev Virtual Phys Prototyp - Proc 5th Int Conf Adv Res Rapid Prototyp 2012:249-54. https://doi.org/10.1201/b11341-40.

[11] Yan C, Hao L, Hussein A, Raymont D. Evaluations of cellular lattice structures manufactured using selective laser melting. Int J Mach Tools Manuf 2012;62:32-8. https://doi.org/10.1016/j.ijmachtools.2012.06.002.

[12] Aremu AO, Maskery I, Tuck C. A comparative finite element study of cubic unit cells for selective laser melting - self-supporting Unit cells, n.d., p. 1238-49.

[13] Zhang X, Huo W, Liu J, Zhang Y, Zhang S, Yang J. 3D printing boehmite gel foams into lightweight porous ceramics with hierarchical pore structure. J Eur Ceram Soc 2019. https://doi.org/10.1016/j.jeurceramsoc.2019.10.032.

[14] Kulka J, Mantic M, Fedorko G, Molnar V. Analysis of crane track degradation due to operation. Eng Fail Anal 2016;59:384-95. https://doi.org/10.1016/j.engfailanal. 2015.11.009.

[15] Kohnen P, Haase C, Bultmann J, Ziegler S, Schleifenbaum JH, Bleck W. Mechanical properties and deformation behavior of additively manufactured lattice structures of stainless steel. Mater Des 2018;145:205-17. https://doi.org/10.1016/j.matdes. 2018.02.062.

[16] Lozanovski B, Leary M, Tran P, Shidid D, Qian M, Choong P, et al. Computational modelling of strut defects in SLM manufactured lattice structures. Mater Des 2019;171:107671https://doi.org/10.1016/j.matdes.2019.107671.

[17] Lang Y, Tian C, Dai X, Wang C. Preparation of YSZ porous ceramics with precise porosity control. Int J Appl Ceram Technol 2019:1-6. https://doi.org/10.1111/ijac. 13431.

[18] Sadowski T, Samborski S. Modeling of porous ceramics response to compressive loading. J Am Ceram Soc 2003;86:2218-21. https://doi.org/10.1111/jM151-2916. 2003.tb03637.x.

[19] Sadowski T, Samborski S. Prediction of the mechanical behaviour of porous ceramics using mesomechanical modelling. Comput Mater Sci 2003;28:512-7. https:// doi.org/10.1016/j.commatsci.2003.08.008.

[20] Sadowski T, Samborski S. On the different behaviour of porous ceramic polycrystalline materials under tension and compression stress state. Comput Fluid Solid Mech 2003;2003:615-8. https://doi.org/10.1016/B978-008044046-0.50151-2.

[21] Samborski S, Sadowski T. A new micromechanics based predictive method for porous ceramics behaviour under compression. Brittle Matrix Compos 2007;8:507-16. https://doi.org/10.1533/9780857093080.507.

[22] Sadowski T, Samborski S. Development of damage state in porous ceramics under compression. Comput Mater Sci 2008;43:75-81. https://doi.org/10.1016/j. commatsci.2007.07.041.

[23] Kubiak T, Samborski S, Teter A. Experimental investigation of failure process in compressed channel-section GFRP laminate columns assisted with the acoustic emission method. Compos Struct 2015;133:921-9. https://doi.org/10.1016/j. compstruct.2015.08.023.

[24] Tandon N, Choudhury A. Review of vibration and acoustic measurement methods for the detection of defects in rolling element bearings. Tribol Int 1999;32:469-80. https://doi.org/10.1016/S0301-679X(99)00077-8.

[25] Tandon N, Nakra BC. Comparison of vibration and acoustic measurement techniques for the condition monitoring of rolling element bearings. Tribol Int 1992;25:205-12. https://doi.org/10.1016/0301-679X(92)90050-W.

[26] Chan YC, Shintani K, Chen W. Robust topology optimization of multi-material lattice structures under material and load uncertainties. Front Mech Eng 2019;14:141-52. https://doi.org/10.1007/s11465-019-0531-4.

[27] Li YC, Zhang J, Lin HQ. Topological phase and lattice structures in spin-chain models. Phys Rev B 2019;99:205424https://doi.org/10.1103/PhysRevB.99. 205424.

[28] Jin N, Wang F, Wang Y, Zhang B, Cheng H, Zhang H. Failure and energy absorption characteristics of four lattice structures under dynamic loading. Mater Des 2019;169:107655https://doi.org/10.1016/j.matdes.2019.107655.

[29] Geng X, Lu Y, Liu C, Li W, Yue Z. Fracture characteristic analysis of cellular lattice structures under tensile load. Int J Solids Struct 2019;163:170-7. https://doi.org/ 10.1016/j.ijsolstr.2019.01.006.

[30] Samborski S, Sadowski T. Dynamic fracture toughness of porous ceramics. J Am Ceram Soc 2010;93:3607-9. https://doi.org/10.1111/j.1551-2916.2010.04133.x.

[31] Zargarian A, Esfahanian M, Kadkhodapour J, Ziaei-Rad S, Zamani D. On the fatigue behavior of additive manufactured lattice structures. Theor Appl Fract Mech 2019;100:225-32. https://doi.org/10.1016Zj.tafmec.2019.01.012.

[32] Instytut Metalurgii Żelaza. Zwick/Roell Z100 testing machine for tests at elevated temperature up to 1200°C n.d. http://www.imz.pl/en/news/BL Department_of_ Investigations_of_Properties/Zwick_Roell_Z100_testing_machine_for_tests_at/[30, 232,,,,].